Thermodynamic geometry of supercooled water

Helge-Otmar May
University of Applied Sciences, Darmstadt, Germany

Peter Mausbach
Cologne University of Applied Sciences, Cologne, Germany

George Ruppeiner
Division of Natural Sciences, New College of Florida, Sarasota, Florida USA
(Received 15 November 2014; published 26 March 2015)

The thermodynamic curvature scalar R is evaluated for supercooled water with a two-state equation of state correlated with the most recent available experimental data. This model assumes a liquid-liquid critical point. Our investigation extends the understanding of the thermodynamic behavior of R considerably. We show that R diverges to $-\infty$ when approaching the assumed liquid-liquid critical point. This limit is consistent with all of the fluid critical point models known so far. In addition, we demonstrate a sign change of R along the liquid-liquid line from negative near the critical point to positive on moving away from the critical point in the low density "ice-like" liquid phase. We also trace out the Widom line in phase space. In addition, we investigate increasing correlation length in supercooled water and compare our results with recent published small angle x-ray scattering measurements.

DOI: 10.1103/PhysRevE.91.032141 PACS number(s): 51.30.+i, 61.20.−p, 05.70.−a, 64.60.−i

I. INTRODUCTION

The thermodynamic Riemann scalar curvature R is an element of thermodynamic metric geometry [1]. R reveals information about intermolecular interactions [2] and the size of organized mesoscopic structures [3]. By applying thermodynamic fluctuation theory [4], R can be formulated as an invariant for any thermodynamic coordinate system. In the recent past, this geometric concept has been systematically developed for atomic and molecular fluid systems using thermodynamic data obtained from experiments and computer simulations [5–10]. These studies take us a long way toward completing the picture of R in fluid and solid systems. Moreover, these investigations reveal interesting features that may bear important information for the ongoing effort of understanding the thermodynamic curvature scalar R in a broader context of thermodynamic systems, including black hole thermodynamics [3,11].

Recently, the analysis of thermodynamic curvature R in the whole fluid phase was examined for four fluids based on equations of state (EOS) obtained by correlation with experimental data [10]. In this study, R diagrams were constructed for argon, hydrogen, carbon dioxide, and water. All four fluids exhibit significant regimes of positive R at very high pressure in the supercritical regime similar to the LJ fluid [9]. Water is special in having, in addition, a slab-like feature of positive R in the stable liquid phase near the triple point, and encompassing the density maximum at 4 °C and ambient pressure. Based on experimental findings [12–14] the $R > 0$ slab can be associated with an onset of hydrogen-bond (HB) clustering of open "ice-like" structures within the HB network [10,15]. This connects to our work since it was proposed [10] that solid-like properties reveal themselves thermodynamically through positive values of the thermodynamic curvature R.

Near the critical point, $|R|$ is expected to be proportional to the correlation volume ξ^d, where d is the spatial dimensionality of the system. To evaluate the dimensionless proportionality constant between $|R|$ and ξ^d near the critical point, model calculations in which both R and ξ are evaluated are required. Several calculations of this type have been carried out in critical regions: (1) four pure fluids near the critical point [1], (2) the one-dimensional ferromagnetic Ising model [16], (3) the one-dimensional Takahashi gas [17], and a decorated Ising chain [18]. In all these cases, the same proportionality constant was obtained:

$$\xi^d = \frac{|R|}{2}, \tag{1}$$

with $R < 0$ in each case. Based on these limited calculations, the proportionality constant $\frac{1}{2}$ would appear to be universal but there is yet no general proof.

Water is unique among other pure fluids we have looked at in having dramatically decreasing R, to negative values, on cooling into the metastable liquid phase. This is of interest because anomalies apparent in stable cold liquid water become increasingly pronounced in the metastable supercooled state. In this study, we extend our investigations of R [10] into the metastable supercooled liquid water regime. In addition, the application of Riemannian geometry on unusual phase diagrams of the type here may critically test the findings made for ordinary substances and may give additional insights into the thermodynamic behavior of R.

Various scenarios have been proposed to explain the anomalous behavior of supercooled water [19–21]. A scenario that has attracted much attention employs the assumption of a liquid-liquid phase transition (LLT) terminated at a liquid-liquid critical point (LLCP) [20]. This scenario shows how water anomalies could be linked to critical point fluctuations. Figure 1 shows a schematic diagram [22] of metastable supercooled liquid water with a LLCP.

The purpose of this article is the analysis of the thermodynamic curvature R in the context of the LLCP scenario by using a theoretical model (EOS) consistent with experimental data

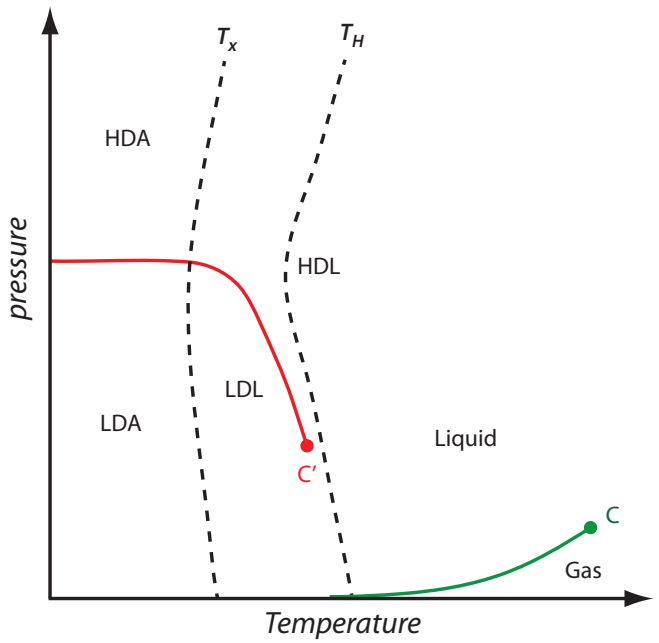

FIG. 1. (Color online) A schematic diagram of the metastable, supercooled liquid phase extending down to the limiting homogeneous nucleation temperature T_H, where an amorphous solid must form. We show the first-order liquid-liquid phase transition curve between a high-density phase (HDL) and a low-density phase (LDL). This curve terminates in a second critical point C′. This phase transition is not directly accessible to measurements in the bulk, since it falls below T_H. However, the thermodynamic properties in the liquid phase appear to be strongly affected by the critical properties near C′. Further metastable and regular cooling brings us to the cubic ice crystallization curve T_x, with amorphous high-density and low-density amorphous phases HDA and LDA corresponding to the HDL and LDL liquid phases. Also shown is the regular liquid-vapor coexistence line, terminating in the regular critical point C.

[23]. We attempt no final conclusion concerning the existence of a LLCP. Such a point must be demonstrated experimentally. A detailed discussion of the pros and cons regarding the LLCP scenario, and a review of currently available experimental data, may be found elsewhere [24–27].

An important issue in this paper is the sign of R. In this respect, a key early result [28,29] was the finding that for the ideal Fermi (Bose) gasses, with the effective intermolecular quantum statistical interaction being repulsive (attractive), the sign of R is uniformly positive (negative). The midpoint between these quantum cases is the classical ideal gas, with $R = 0$ [1]. Our previous results in fluids [9,10] support this correspondence between the sign of R and the basic character of the intermolecular interactions, even for the condensed liquid and solid regimes, where $|R|$ is generally found to be small, on the order of the molecular volume.

The liquid state in water has mostly negative R, because the water molecules are mostly far enough apart that the attractive interaction dominates. Likewise, if the LLCP is in the same universality class as that of the 3D Ising model, as is generally assumed, R should be negative everywhere in the critical regime. There are some cases, however, where positive R in liquid water might be expected. It is thought that the source of a number of liquid water's anomalies are tetragonal solid-like structures mediated by hydrogen bonding. We have proposed [10] that in the *stable* liquid, R identifies the presence of these solid-like structures by becoming positive. We propose here that this idea extends into the metastable water regime. Tetragonal "ice-like" structures generally take up more space than the more disorganized liquid structures. Hence, we would look for positive R particularly in relatively low-density liquids (LDL). We find a transition to positive R in the LDL phase along the liquid-liquid coexistence curve.

Our paper is organized as follows. First, we analyze and discuss the thermodynamic curvature scalar in the supercooled water region, using in particular an R diagram. We strengthen the motivation for the choice of the EOS used for this purpose. Furthermore, we find consistency with R calculated from earlier results obtained in the stable cold water state [10]. We follow with a discussion of the asymptotic behavior of the thermodynamic curvature close to the LLCP. We key also on the location of the Widom line corresponding to curves of maximum $|R|$ at either constant pressure or constant temperature. Furthermore, we investigate increasing correlation length in supercooled water calculated from the thermodynamic curvature and compare the results with those determined from small angle x-ray scattering measurements [30].

II. ANALYSIS AND DISCUSSION

The anomalous behavior of several thermodynamic properties of metastable supercooled water has motivated various attempts at theoretical explanation [19–21]. Almost all models propose the existence of two different states of local molecular order, namely a high-density liquid (HDL) and a low-density liquid (LDL) structure. HDL configurations are favored at higher temperatures and higher pressures, where the local tetrahedrally coordinated HB network structure is not fully developed. LDL structures are favored at lower temperatures and lower pressures, where open "ice-like" HB network configurations develop. It is believed that the competition between these two configurations generates the anomalies in the thermodynamic response functions of cold and supercooled water.

EOS's based on the proposed existence of two different states of local molecular order have provided significantly improved accuracy for the thermodynamic properties of supercooled water. In a series of papers, so-called two states EOS (TSEOS) models were developed by Holten *et al.*, and correlated with both experimental [23,27,31–33] and computer simulation [34,35] data. Holten *et al.* assumed that liquid water at low temperatures can be described as a mixture of two interconvertible structures, a HDL state and a LDL state whose ratio is controlled by thermodynamic equilibrium. Incorporating the LLCP, Holten *et al.* [33] developed an EOS that allows the use of a curved LLT, in contrast to previous models that worked with a straight LLT line [31,32]. A refined equation [23] based on this correlation [33] represents almost all the thermodynamic data of cold and supercooled water. Because we are interested in connecting smoothly the thermodynamic curvature obtained in the supercooled metastable state to our findings of cold stable water [10] we use the parameter set of Ref. [23] in our analysis. In a very

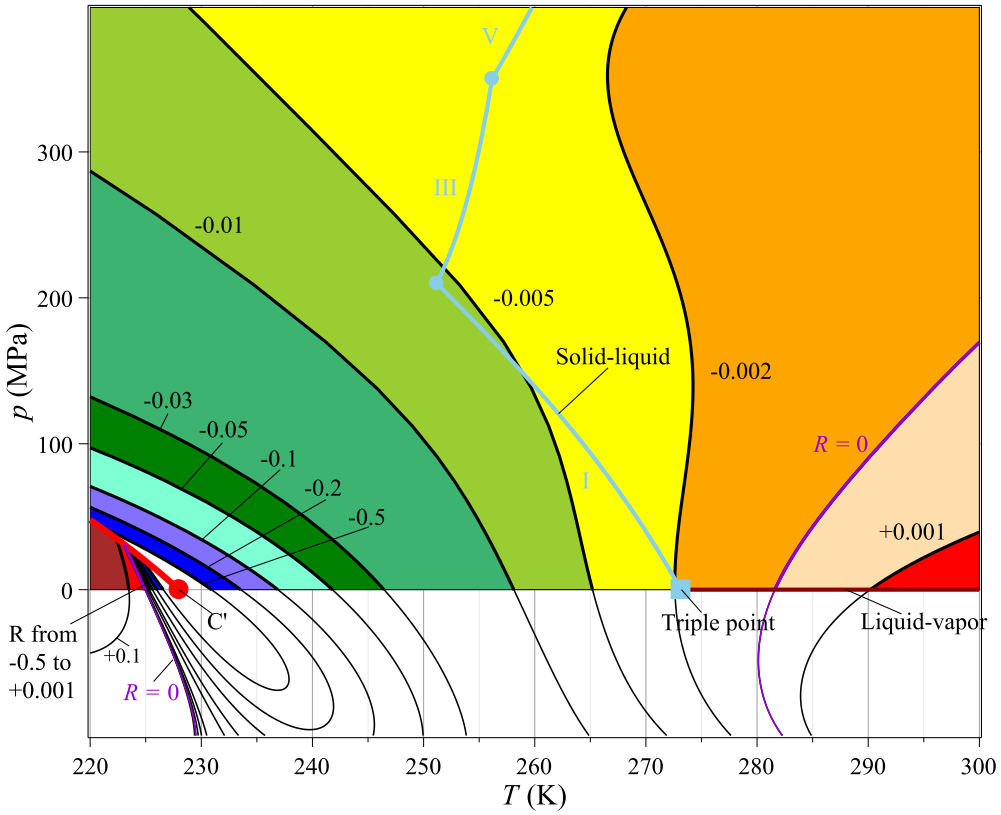

FIG. 2. (Color online) R diagram (R contours measured in nm^3) of supercooled water for temperatures ranging from $T = 220$ to 300 K and for pressures ranging from $p = -100$ to 400 MPa. In the negative pressure region we omit a colored contour field in order to indicate the extrapolated character of this region. The LLT line is marked by a red solid curve terminating at the LLCP marked by a red solid circle (C′). Two lines $R = 0$ develop in the diagram, one in the stable cold water region close to the freezing line, and the other in the LDL region below the LLT line. The triple point is marked by a blue solid box, and the solid-liquid coexistence line by a blue solid curve showing the melting lines of ice I, III, and V. The liquid-vapor coexistence curve starting from the triple point is indicated as a dark red line.

recent study [27], the model of Ref. [23] has been evolved further but this does not affect our conclusions.

A brief outline of the procedure of determining R in the two cases of (T,ρ) and (T,p) coordinates is given in Appendix A. Since R is a thermodynamic invariant, its value for a particular thermodynamic state does not depend on the coordinates employed to calculate it. In Appendix B, a brief outline of the mathematical structure of the TSEOS model [23] is given. Because this model is naturally expressed in terms of the Gibbs energy G, the calculation of R differs from that in recent studies [9,10], where (T,ρ) coordinates were used. By using the Gibbs energy as the decisive thermodynamic potential, the metric elements have to be formulated in (T,p) coordinates [6].

A. Thermodynamic curvature from the Holten-Anisimov-Sengers EOS

The HAS-TSEOS model [23] of Holten, Anisimov, and Sengers (HAS) was fit to experimental data ranging from the homogeneous ice nucleation temperature up to 300 K and from a pressure up to 400 MPa. Because our interest concentrates on the qualitative behavior of R in the supercooled region we use this equation to extrapolate data into regions around the assumed LLCP, including negative pressures. We assume that the HAS-TSEOS predicts this region at least qualitatively with their choice of LLCP coordinates of $T_C = 228$ K and $p_C = 0$ MPa.

In Fig. 2 we present the R diagram (R contours) of supercooled water for temperatures ranging from $T = 220$ to 300 K and for pressures ranging from $p = -100$ to 400 MPa. The LLT line is marked by a red solid curve terminating at the LLCP marked by a red solid circle and denoted by C′. In the negative pressure region of Fig. 2 we omitted a colored contour field in order to indicate its extrapolated character. Starting in the stable cold water phase the thermodynamic curvature R is positive and consistent with our previous reported findings [10]. Cooling the system isobarically into the supercooled state leads to negative and decreasing R corresponding to increasing isothermal compressibility k_T. The sign change of R along the line $R = 0$ occurs in the stable cold liquid phase close to the freezing line, as shown in Ref. [10]. At the assumed LLCP, R diverges to $-\infty$ consistent with all of the fluid critical point models known so far [3]. Furthermore, a general feature of R contours found in other critical point models of fluids is also fulfilled for the LLCP of supercooled water. Close to the LLCP, the R contours begin and end on the LLT line (i.e., see the $R = -0.5$ contour in Fig. 2), and loop around the LLCP, establishing a distinct, self-contained, critical point regime. More interestingly, the thermodynamic curvature R remains negative for higher pressures above the LLT line consistent with the HDL structure, whereas an additional line $R = 0$

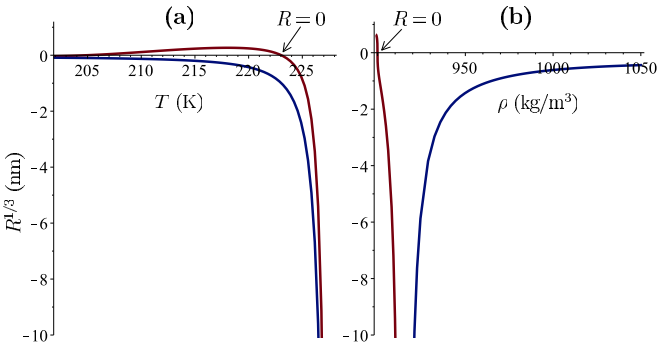

FIG. 3. (Color online) Cube root of the thermodynamic curvature $R^{1/3}$ along the LDL side (red curve) and the HDL side (blue curve) of the LLT line as a function of temperature (a) and of density (b). On the LDL side a point $R = 0$ occurs approximately at $T = 223$ K and $\rho = 900$ kg/m^3 (marked by arrows) indicating a change to organized "ice-like" structures.

develops at lower pressures below the LLT line with large regions of positive R, indicating the more ordered "ice-like" structure of the LDL phase. This point becomes clearer if the thermodynamic curvature R is plotted along the LLT line.

In Fig. 3 we show the cube root of thermodynamic curvature $R^{1/3}$ along the LDL side (red curve) and the HDL side (blue curve) of the LLT line as a function of temperature (a) and of density (b). We scale the thermodynamic curvature as $R^{1/3}$ because this quantity measures directly the correlation length ξ (see Sec. II B). Both Figures show nicely strong diverging $R^{1/3}$ to $-\infty$ at the LLCP with $T_C = 228$ K and $\rho_C = 914.844$ kg/m^3. On the HDL side (blue curve) the thermodynamic curvature remains negative characterizing disorganized liquid structures, whereas on the LDL side (red curve) a zero crossing point occurs approximately at $T = 223$ K and $\rho = 900$ kg/m^3 (marked by arrows), indicating a change to organized "ice-like" structures.

A good validation of our calculated R would be a smooth connection to the thermodynamic curvature calculated in the stable liquid phase above the melting curve [10] based on the IAPWS-95 formulation [36,37]. In Fig. 4, we show the temperature dependence of the thermodynamic curvature R ranging from $T = 240$ to 330 K at different constant pressures of $p = 300, 200, 100, 60, 20$, and 0.1 MPa. The thermodynamic curvatures based on the IAPWS-95 formulation are shown as green lines, whereas the red lines show the thermodynamic curvatures based on the HAS-TSEOS. Both curves exhibit a smooth connection without significant discontinuities at the point of switching. Strictly speaking, the boundary of the range of validity of IAPWS-95 is the melting curve. However, when extrapolating the data from the IAPWS-95 formulation into the supercooled region at $p = 0.1$ MPa, the thermodynamic curvature follows closely that of the HAS-TSEOS. An increase in pressure results in decreasing compliance at low temperatures. At a pressure of $p = 300$ MPa the two curves match only for temperatures of roughly $T > 300$ K, where the thermodynamic curvature obtained from the IAPWS-95 formula develops an unrealistic

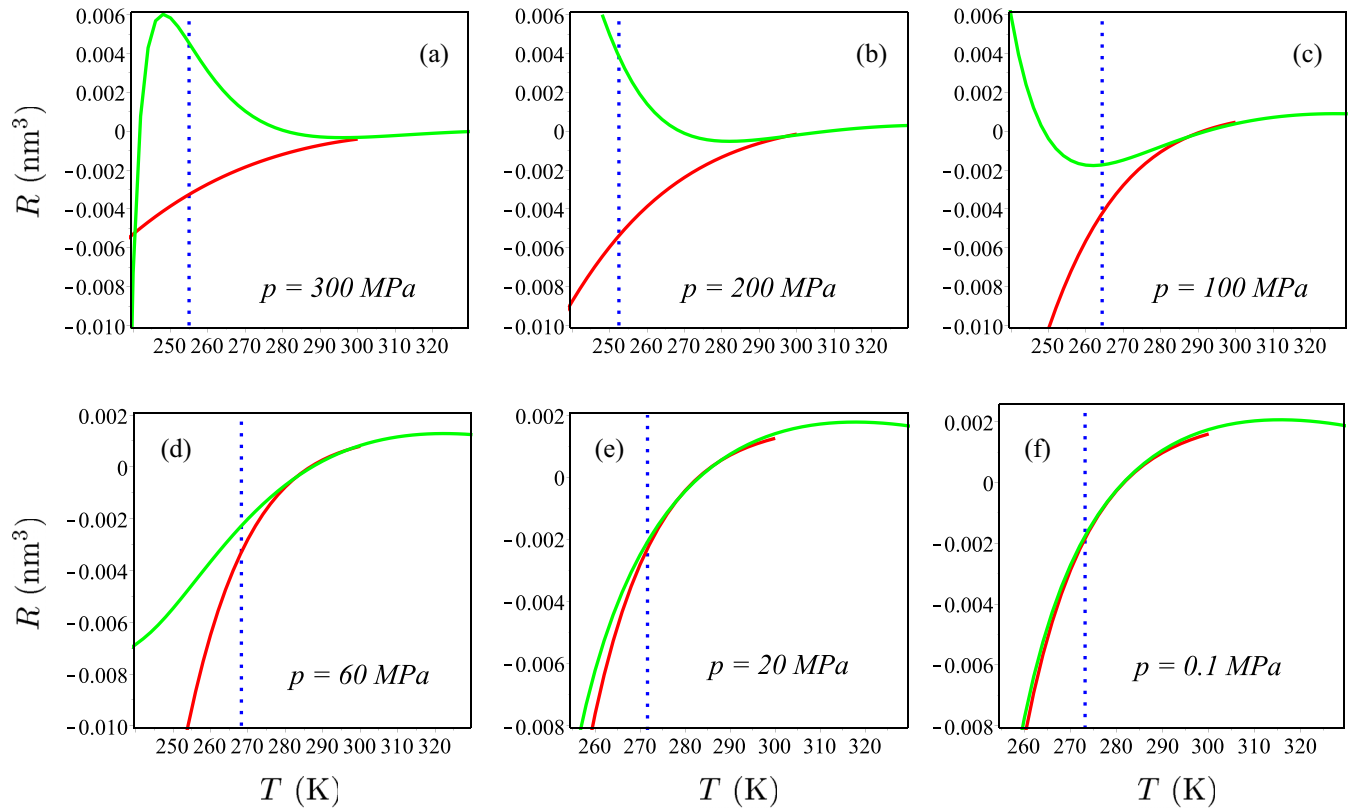

FIG. 4. (Color online) Comparison between the thermodynamic curvature R (measured in nm^3) obtained from the HAS-TSEOS (red lines) [23] and the IAPWS-95 formulation (green lines) [36,37] for temperatures ranging from $T = 240$ to 330 K at different constant pressures of $p = 300, 200, 100, 60, 20$, and 0.1 MPa. The blue dotted lines indicate the melting temperatures.

extrema. Generally, the R data are pretty consistent down to the melting temperature at low pressures, less so at high pressures. This is consistent with the description of Holten *et al.* who also find larger density deviations between HAS-TSEOS and IAPWS-95 at higher pressures [23]. Nevertheless, both formulations clearly confirm the findings of positive R in stable cold water near the triple point and the disappearance of the $R > 0$ slab for pressures $p > 200$ MPa [10]. We add that the smooth connection of thermodynamic curvature is a strong indication for the high precision of both EOSs in the range of its applicability, especially because the calculation method for the thermodynamic curvature is different for the two EOSs. The Helmholtz free energy is the thermodynamic potential used with (T,ρ) coordinates in the stable cold water phase, whereas the Gibbs free energy with (T,p) coordinates is used for the metastable supercooled region.

In summary, the overall behavior of the thermodynamic curvature R nicely confirms the picture developed in the stable fluid [10] in the supercooled water regime. The sign change of R along the LLT line indeed corresponds to the two liquid phases (HDL and LDL) along this separation line.

B. Asymptotic behavior of thermodynamic curvature close to the LLCP

A problem that arises within the LLT hypothesis is finding the Widom line [38]. The Widom line is characterized by the locus of points with maximum correlation length ξ either along constant-pressure or constant-temperature paths. Since ξ can be difficult to determine, the Widom line is difficult to find in practice. In place of ξ, extrema in the response functions are regularly used to estimate the course of the Widom line [39] since asymptotically close to critical points all response functions can be expressed in terms of the correlation length. However, our geometrical approach allows a direct computation of the Widom line since the volume of the correlation length is proportional to the Riemannian thermodynamic scalar curvature, $|R| \sim \xi^3$ [5,7]. Investigations for characterizing the Widom line were carried out in the supercritical state of the van der Waals and the LJ system along constant pressure and constant-temperature paths [5,7]. These studies show clearly that response function extrema do not always follow the Widom line and they vary considerably when departing from the critical point. Under these circumstances, it is of great interest to calculate the Widom line for the LLCP in supercooled water based on the maximum of the scalar curvature $|R|_{\max}$.

In Fig. 5, we show the development of negative curvature R near the LLCP along constant pressure [Fig. 5(a)] and constant temperature paths [Fig. 5(b)]. According to the critical behavior of the correlation length ξ, the $-R$ curves diverges to ∞ when approaching the assumed LLCP at $p_C = 0$ MPa, $T_C = 228$ K, and $\rho_C = 914.844$ kg/m^3 and they develop pronounced maxima when applying negative pressure [Fig. 4(a)] or decreasing the temperature [Fig. 5(b)].

Points with maximum $|R|$ determine the loci of correlation length maxima, e.g., the Widom line. In Fig. 6, we show the slope of $|R|_{\max}$ at constant temperature and constant pressure in the $\rho - T$ [Fig. 6(a)] and the $p - T$ [Fig. 6(b)] phase projections. In Fig. 6(a), the lines of $|R|_{\max}$ start at the LLCP

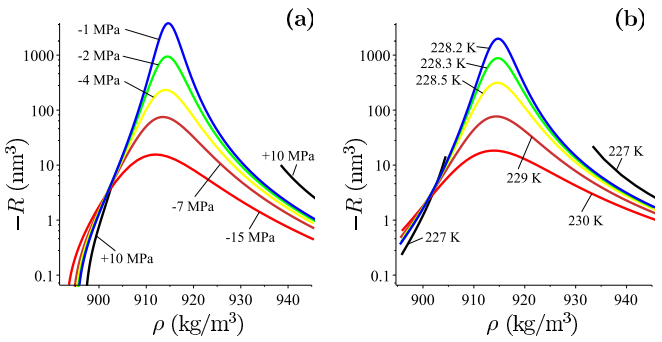

FIG. 5. (Color online) Development of the negative curvature R near the LLCP along isobars (a) in a range from -15 to 10 MPa and along isotherms (b) ranging from 227 to 230 K. LLCP coordinates are $p_C = 0$ MPa, $T_C = 228$ K, and $\rho_C = 914.844$ kg/m^3.

with different negative gradients. The course of both lines of maximum curvature correspond to an increase in temperature with density decrease, but $|R|_{\max}$ at constant temperature (red curve) passes through an extrema at $\rho \approx 909$ kg/m^3 followed by an increase in temperature with density increase. In Fig. 6(b), the lines of $|R|_{\max}$ start with roughly the same negative gradient at the LLCP and both curves correspond to an increase in temperature with negative pressure increase, where the increase in temperature is stronger for $|R|_{\max}$ at constant temperature (red curve). For the LLCP of supercooled water we confirm the findings made elsewhere [7] that the lines of $|R|_{\max}$ at constant temperature or constant pressure widens rapidly upon departure from the LLCP that should be of some importance in determining the position of the LLCP.

In a recent study, Huang *et al.* [30] demonstrated that the correlation length ξ of bulk liquid water determined by small angle x-ray scattering measurements rises rapidly upon supercooling. The lowest accessible temperature in this study, $T = 252$ K, was set by beam-induced crystallization. The authors were able to fit the correlation length using a power law as

$$\xi = \xi_0\, \varepsilon^{-\nu}, \tag{2}$$

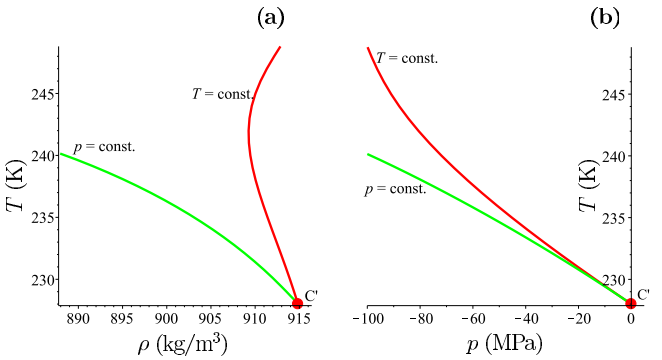

FIG. 6. (Color online) Points with maximum $|R|$ along curves with constant temperature or pressure determining the Widom line. The slope of lines $|R|_{\max}$ is shown at constant temperature and constant pressure in the $\rho - T$ (a) and the $p - T$ (b) phase projections. The lines of $|R|_{\max}$ start at the LLCP with $p_C = 0$ MPa, $T_C = 228$ K, and $\rho_C = 914.844$ kg/m^3.

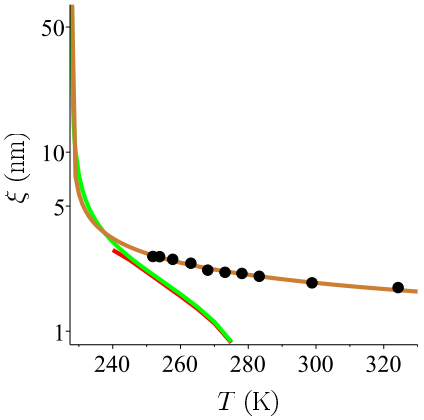

FIG. 7. (Color online) Temperature-dependent behavior of the correlation length ξ, at ambient pressure in the supercooled region of water. Circles indicate small angle x-ray scattering measurements [30] down to a temperature of 252 K. The brown curve represents their power law [30] extrapolated to values close to the LLCP. The green and the red curve show ξ calculated using the relation $|R|/2 = \xi^3$ obtained from the HAS-TSEOS [23] and the IAPWS-95 formula [36], respectively.

where $\varepsilon = \frac{T}{T_W} - 1$, with $\xi_0 = 1.287$ Å, $\nu = 0.32$, and a Widom line temperature of $T_W = 228$ K at constant ambient pressure. This form of the power law behavior has been used to phenomenologically describe the thermodynamic anomalies of supercooled water [40]. Since the reported measurements [30] are far from the conjectured second critical point in water, the exponent $\nu = 0.32$ is thus not expected to coincide with the critical exponent $\nu = 0.629$ for the 3D Ising model, a value confirmed for liquid-liquid critical points by recent computer simulations, analyzed with finite-scaling theory [41].

It is of great interest to compare the postulated universal law Eq. (1) in the vicinity of the LLCP of water with the power law results according to Eq. (2). In Fig. 7, we show the temperature-dependent behavior of ξ at ambient pressure in the supercooled region of water. Circles indicate the measurements of Huang *et al.* down to a temperature of 252 K, and the brown curve represents their power law extrapolated to values close to the LLCP. The green curve shows the calculated correlation length from Eq. (1) obtained from the HAS-TSEOS, whereas the red line is evaluated from the IAPWS-95 formula. The results indicate that water anomalies can be attributed to an increasing characteristic length scale of density fluctuation between HDL and LDL regions. Within uncertainties of both, small angle x-ray scattering measurements [30] and thermodynamic measurements for fitting the HAS-TSEOS [23], the compliance in Fig. 7 is acceptable when approaching the LLCP and supports the universality of the relation $|R|/2 = \xi^3$.

III. CONCLUSION

In this study, we analyzed in detail the behavior of the thermodynamic curvature scalar R in the supercooled water region, using a TSEOS model [23] that presumes the LLCP scenario. We used this equation to extrapolate data into regions around the assumed LLCP expecting, at least, qualitative validity of the equation in this region.

We showed that the basic behavior of R at the LLCP is consistent with the fluid critical point models known so far, including the divergence of R to $-\infty$. Furthermore, the sign change of R along the LLT line confirms findings elsewhere [10], where solid-like fluid states were proposed as corresponding to positive values of R. On the low-pressure LDL side of the LLT line, organized "ice-like" structures lead to positive R, whereas on the high-pressure side HDL structures exhibit only negative curvature. Previously obtained results of positive curvature in stable cold water near the triple point [10] based the IAPWS-95 formula [36] was confirmed on the basis of the TSEOS extended into this region.

Starting from the assumed LLCP we constructed Widom lines corresponding to the locations of maximum $|R|$ along lines of constant pressure and temperature. The lines of $|R|_{\max}$ at constant temperature or constant pressure separate upon departure from the LLCP, indicating that the path used for the calculation of the Widom line is important for determining the location of the LLCP.

Finally, we directly calculated the correlation length from the relation $|R|/2 = \xi^3$ based on the HAS-TSEOS. We compared the calculated correlation length with results obtained from small angle x-ray-scattering measurements and concluded that the postulated universality of Eq. (1) appears to be valid in the context of measurement uncertainties on the LLCP of water.

The LLCP scenario presumed in our study has recently received another interesting point of view [42,43]. By using molecular dynamics studies it was found that bulk water crystallization occurs more rapidly than the equilibration of LDL. Certainly, it is of great interest to investigate the thermodynamic curvature under these circumstances. We are in the process of making a detailed analysis of R for this situation.

ACKNOWLEDGMENTS

We thank Vincent Holten, Monika Thol, and Jadran Vrabec for useful communications. G.R. thanks George Skestos for research support.

APPENDIX A

The thermodynamic line element $d\ell$ is given by the thermodynamic entropy information metric [4]

$$d\ell^2 = \sum_{i,j} g_{ij} dq^i dq^j .$$

$d\ell^2$ is an invariant in the thermodynamic parameters q^i, and the coefficients g_{ij} are the components of the thermodynamic metric tensor. For a one-component fluid there are two independent state variables q^1 and q^2 and the Riemannian curvature is calculated from [6,44]

$$R = -\frac{1}{\sqrt{g}}\left[\frac{\partial}{\partial q^1}\left(\frac{g_{12}}{g_{11}\sqrt{g}}\frac{\partial g_{11}}{\partial q^2} - \frac{1}{\sqrt{g}}\frac{\partial g_{22}}{\partial q^1}\right) + \frac{\partial}{\partial q^2}\left(\frac{2}{\sqrt{g}}\frac{\partial g_{12}}{\partial q^1} - \frac{1}{\sqrt{g}}\frac{\partial g_{11}}{\partial q^2} - \frac{g_{12}}{g_{11}\sqrt{g}}\frac{\partial g_{11}}{\partial q^1}\right)\right],$$

with

$$g = g_{11}\, g_{22} - g_{12}^2.$$

By the rules of Riemannian geometry, the value of the thermodynamic curvature for any thermodynamic state is independent of the coordinate system used to calculate it. If we choose T and ρ as independent variables the basis of our analysis for R is the Helmholtz free energy per volume $a = a(T,\rho)$. (T,ρ) coordinates are orthogonal and therefore [6]

$$g_{12} = g_{T\rho} = 0, \quad g_{11} = g_{TT} = -\frac{1}{k_B T}\frac{\partial^2 a}{\partial T^2},$$

$$g_{22} = g_{\rho\rho} = \frac{1}{k_B T}\frac{\partial^2 a}{\partial \rho^2},$$

where k_B is Boltzmann's constant.

If we choose T and p as independent variables the basis is the Gibbs free energy per volume $\hat{g} = \hat{g}(T,p)$. (T,p) coordinates are not orthogonal and the metric elements become [6]

$$g_{12} = g_{Tp} = -\frac{1}{k_B T}\frac{\partial^2 \hat{g}}{\partial p\, \partial T}, \quad g_{11} = g_{TT} = -\frac{1}{k_B T}\frac{\partial^2 \hat{g}}{\partial T^2},$$

$$g_{22} = g_{pp} = -\frac{1}{k_B T}\frac{\partial^2 \hat{g}}{\partial p^2},$$

$a = a(T,\rho)$ and $\hat{g} = \hat{g}(T,p)$ are calculated from the EOSs discussed in the previous sections and in Appendix B.

APPENDIX B

The HAS-TSEOS [23] assumes that liquid water is a mixture of a HDL structure (index A) and a LDL structure (index B). The model is a member of a large group of TS models that have been applied to thermodynamic phenomena in one-component liquids [45–50]. The fraction of water molecules in state B is denoted by x, and is controlled by a "reaction" A $\leftrightarrow$ B. We start with the Gibbs energy per molecule G and introduce dimensionless quantities:

$$\hat{G} = \frac{G}{R_G T_C}, \quad \hat{T} = \frac{T}{T_C}, \quad \tau = \frac{T - T_C}{T_C}, \quad \pi = \frac{p - p_C}{R_G T_C\, \rho_C},$$

where R_G is the gas constant, and the LLCP parameters are denoted by a subscript C. The equation of state is

$$\frac{\hat{G}}{\hat{T}} = \frac{\hat{G}^A}{\hat{T}} + xL + x\ln x + (1-x)\ln(1-x) + \omega x(1-x),$$

where the field L is given by

$$L = \lambda(\tau + a\pi + b\tau\pi),$$

with the interaction parameter $\omega = 2 + \omega_0\pi$. λ, a, b, and ω_0 are numerical constants. The dimensionless Gibbs energy of the pure component A is given by

$$\hat{G}^A = \sum_{i=1}^{14} c_i \tau^{a_i} \pi^{b_i} + \sum_{i=15}^{20} c_i \tau^{a_i} \pi^{b_i} \exp(-\pi),$$

where c_i, a_i, and b_i are suitable constants. The equilibrium fraction x_e is calculated from the condition

$$\left(\frac{\partial \hat{G}}{\partial x}\right)_{T,p} = 0 \quad \text{at} \quad x = x_e,$$

which yields

$$L + \ln\frac{x_e}{1 - x_e} + \omega(1 - 2x_e) = 0.$$

This equation must be solved numerically for the fraction x_e and the Gibbs free energy is then given as an implicit function from p and T. For the calculation of the Riemann thermodynamic curvature, higher derivatives of the Gibbs free energy have to be calculated, and therefore the derivatives of the fraction $x_e = x_e(T,p)$ have to be calculated numerically as well. This makes the procedure very different from the calculation of the Wagner-Pruß equation, which starts from the Helmholtz free energy in (T,ρ) coordinates and which is given as an explicit function.

[1] G. Ruppeiner, Phys. Rev. A **20**, 1608 (1979).
[2] G. Ruppeiner, Am. J. Phys. **78**, 1170 (2010).
[3] G. Ruppeiner, Springer Proc. Phys. **153**, 179 (2014).
[4] G. Ruppeiner, Rev. Mod. Phys. **67**, 605 (1995); **68**, 313(E) (1996).
[5] G. Ruppeiner, A. Sahay, T. Sarkar, and G. Sengupta, Phys. Rev. E **86**, 052103 (2012).
[6] G. Ruppeiner, Phys. Rev. E **86**, 021130 (2012).
[7] H.-O. May and P. Mausbach, Phys. Rev. E **85**, 031201 (2012).
[8] H.-O. May and P. Mausbach, Phys. Rev. E **86**, 059905(E) (2012).
[9] H.-O. May, P. Mausbach, and G. Ruppeiner, Phys. Rev. E **88**, 032123 (2013).
[10] G. Ruppeiner, P. Mausbach, and H.-O. May, Phys. Lett. A **379**, 646 (2015).
[11] G. Ruppeiner, J. Phys.: Conf. Ser. **410**, 012138 (2013).
[12] F. Mallamace, C. Corsaro, and H. E. Stanley, Sci. Rep. **2**, 993 (2012).
[13] F. Mallamace, C. Corsaro, D. Mallamace, C. Vasi, and H. E. Stanley, Faraday Discuss. **167**, 95 (2013).
[14] F. Mallamace, C. Corsaro, D. Mallamace, S. Vasi, C. Vasi, and H. E. Stanley, J. Chem. Phys. **141**, 18C504 (2014).
[15] H. Tanaka, Eur. Phys. J. E **35**, 113 (2012).
[16] G. Ruppeiner, Phys. Rev. A **24**, 488 (1981).
[17] G. Ruppeiner and J. Chance, J. Chem. Phys. **92**, 3700 (1990).
[18] G. Ruppeiner and S. Bellucci, Phys. Rev. E **91**, 012116 (2015).
[19] R. J. Speedy, J. Phys. Chem. **86**, 982 (1982).
[20] P. H. Poole, F. Sciortino, U. Essmann, and H. E. Stanley, Nature **360**, 324 (1992).
[21] S. Sastry, P. G. Debenedetti, F. Sciortino, and H. E. Stanley, Phys. Rev. E **53**, 6144 (1996).
[22] P. G. Debenedetti and H. E. Stanley, Phys. Today **56**(6), 40 (2003).
[23] V. Holten, M. A. Anisimov, and J. V. Sengers, Technical Report prepared for the International Association for the

Properties of Water and Steam (2012), http://www.iapws.org/minutes/2012/Holten2012-report.pdf
[24] P. G. Debenedetti, J. Phys.: Condens. Matter **15**, R1669 (2003).
[25] J. C. Palmer, F. Martelli, Y. Liu, R. Car, A. Z. Panagiotopoulos, and P. G. Debenedetti, Nature **510**, 385 (2014).
[26] S. L. Meadley and C. A. Angell, *Proceedings of the International School of Physics "Enrico Fermi"* Course CLXXXVII (unpublished) (2014).
[27] V. Holten, J. V. Sengers, and M. A. Anisimov, J. Phys. Chem. Ref. Data **43**, 043101 (2014).
[28] H. Janyszek and R. Mrugała, J. Phys. A: Math. Gen. **23**, 467 (1990).
[29] H. Oshima, T. Obata, and H. Hara, J. Phys. A: Math. Gen. **32**, 6373 (1999).
[30] C. Huang, T. M. Weiss, D. Nordlund, K. T. Wikfeldt, L. G. M. Pettersson, and A. Nilsson, J. Chem. Phys. **133**, 134504 (2010).
[31] V. Holten, C. E. Bertrand, M. A. Anisimov, and J. V. Sengers, J. Chem. Phys. **136**, 094507 (2012).
[32] V. Holten, J. Kalov, M. A. Anisimov, and J. V. Sengers, Int. J. Thermophys. **33**, 758 (2012).
[33] V. Holten and M. A. Anisimov, Sci. Rep. **2**, 713 (2012).
[34] V. Holten, D. T. Limmer, V. Molinero, and M. A. Anisimov, J. Chem. Phys. **138**, 174501 (2013).
[35] V. Holten, J. C. Palmer, P. H. Poole, P. G. Debenedetti, and M. A. Anisimov, J. Chem. Phys. **140**, 104502 (2014).
[36] W. Wagner and A. Pruß, J. Phys. Chem. Ref. Data **31**, 387 (2002).
[37] NIST Chemistry WebBook, http://webbook.nist.gov/chemistry/.
[38] J. Luo, L. Xu, E. Lascaris, H. E. Stanley, and S. V. Buldyrev, Phys. Rev. Lett. **112**, 135701 (2014).
[39] L. Xu, P. Kumar, S. V. Buldyrev, S.-H. Chen, P. H. Poole, F. Sciortino, and H. E. Stanley, Proc. Natl. Acad. Sci. USA **102**, 16558 (2005).
[40] H. Kanno and C. A. Angell, J. Chem. Phys. **70**, 4008 (1979).
[41] P. Gallo and F. Sciortino, Phys. Rev. Lett. **109**, 177801 (2012).
[42] E. B. Moore and V. Molinero, J. Chem. Phys. **132**, 244504 (2010).
[43] E. B. Moore and V. Molinero, Nature **479**, 506 (2011).
[44] I. S. Sokolnikoff, *Tensor Analysis* (Wiley, New York, 1951).
[45] E. J. Rapoport, J. Chem. Phys. **46**, 2891 (1967); **48**, 1433 (1968).
[46] E. G. Ponyatovsky, V. V. Sinitsyn, and T. A. Pozdnyakova, J. Chem. Phys. **109**, 2413 (1998).
[47] I. L. Aptekar and E. G. Ponyatovsky, Fiz. Met. Metalloved. **25**, 777 (1968).
[48] H. Tanaka, Europhys. Lett. **50**, 340 (2000); J. Chem. Phys. **112**, 799 (2000).
[49] C. A. Angell, C. T. Moynihan, and M. Hemmati, J. Non-Cryst. Solids **274**, 319 (2000).
[50] M. J. Cuthbertson and P. H. Poole, Phys. Rev. Lett. **106**, 115706 (2011).